Carrier localization mechanisms in $In_xGa_{1-x}N$/GaN quantum wells

D. Watson-Parris,[*] M. J. Godfrey, and P. Dawson
School of Physics and Astronomy, University of Manchester, Manchester M13 9PL, United Kingdom

R. A. Oliver, M. J. Galtrey, M. J. Kappers, and C. J. Humphreys
Department of Materials Science and Metallurgy, University of Cambridge, Pembroke Street, Cambridge CB2 3QZ, United Kingdom
(Received 7 June 2010; revised manuscript received 14 January 2011; published 16 March 2011)

Localization lengths of the electrons and holes in InGaN/GaN quantum wells have been calculated using numerical solutions of the effective mass Schrödinger equation. We have treated the distribution of indium atoms as random and found that the resultant fluctuations in alloy concentration can localize the carriers. By using a locally varying indium concentration function we have calculated the contribution to the potential energy of the carriers from band gap fluctuations, the deformation potential, and the spontaneous and piezoelectric fields. We have considered the effect of well width fluctuations and found that these contribute to electron localization, but not to hole localization. We also simulate low temperature photoluminescence spectra and find good agreement with experiment.

DOI: 10.1103/PhysRevB.83.115321 PACS number(s): 73.20.Fz, 73.21.Fg, 77.65.Ly

Despite the relatively high dislocation density in InGaN/GaN quantum well (QW) structures grown on *c*-plane sapphire, the room temperature photoluminescence (PL) efficiency of such QWs can be very high.[1] This is generally attributed to localization of the carriers which reduces the effect of nonradiative recombination at the dislocations.[2–4] The precise nature of this localization is still however a matter of debate. Three possible causes of carrier localization that have been widely cited are well width fluctuations,[5–7] random alloy fluctuations[8] including In-N-In chains,[9] and indium clustering.[10,11] Smeeton *et al.* have shown however that gross indium clustering observed in TEM images of InGaN QWs can be caused by electron beam damage.[12]

In this work we present the results of theoretical calculations which demonstrate the importance of random fluctuations in alloy composition, and of well width fluctuations. Previous theoretical work on carrier localization has considered the properties of bulk InGaN with or without embedded InGaN quantum dots (QDs).[13,14] Using an atomistic empirical pseudopotential method they found that in bulk zinc blende InGaN hole wave functions are localized by alloy fluctuations alone, and that the electron wave functions required a dot, or cluster-like confinement, to be localized. The properties of these bulk zinc-blende materials are expected to differ from those in the wurtzite QW structures we consider because of the effect of the large strain, and piezoelectric field across the QW in the case of wurtzite materials.

Our method is to calculate the potential energy landscape of the QW using a random distribution of indium atoms. Once we have calculated this potential energy we solve the effective mass Schrödinger equation using the finite difference approximation to find the energy eigenvalues and wave functions of the carriers. Performing this calculation for different distributions of indium atoms and averaging the results reveals the mean localization lengths for electrons and holes.

Experimental results showing the random nature of the indium distribution and the occurrence of well width fluctuations are described in Sec. I. Our calculations of the carrier potential energy and the subsequent solution of the Schrödinger equation are described in Sec. II, and the results of these calculations are discussed in Sec. III.

I. MICROSTRUCTURAL DATA

In order to model the localization of carriers in InGaN QWs, a realistic description of their nanoscale structure is required. Here, we base our model on the experimental data of InGaN QWs gained by Galtrey *et al.*[15,16] using atom probe tomography (APT). APT has two major advantages over conventional transmission electron microscopy (TEM) studies of InGaN QW microstructures: First, the three-dimensional nature of the APT data set is more appropriate to the development of a three-dimensional model than the two-dimensional projections usually recorded in TEM, and second, the high energy electron beam used in TEM has been reported[12] to rapidly damage InGaN QWs, resulting in potentially unreliable structural data. We will outline the key results of APT studies of InGaN quantum wells grown at a single temperature, and highlight the specific features of the APT data set that we have used as an input to our model.

For quantum wells grown at a single temperature, with $x = 0.18$ and 0.25, the APT data revealed the $In_xGa_{1-x}N$ within the quantum well to be a random alloy.[12] The experimentally determined distribution of indium atoms within the quantum well was compared to the expected binomial distribution for a random alloy. Figure 1 shows this comparison for a typical $x = 0.25$ quantum well sample. A χ^2 test was used to assess whether there was any statistically significant deviation from the random distribution, but no evidence was found for any indium clustering.[15] Hence, in our calculations, the InGaN within the QW has been modeled as having a random, uncorrelated indium distribution.

Further APT studies[16] revealed important information regarding the two QW interfaces. We describe the interface in which the InGaN is grown on the GaN as the lower interface and the interface at which the InGaN is capped with more GaN as the upper interface. The lower interface was found to be both smooth and abrupt. In contrast, the upper interface was

 ©2011 American Physical Society

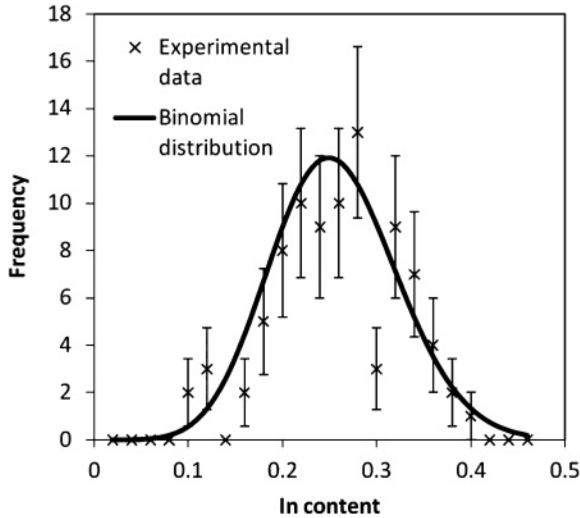

FIG. 1. Statistical analysis of the distribution of indium contents in InGaN QWs indicates no deviation from that expected in a random alloy. For the composition frequency distributions shown here, APT data from green-emitting QW material was divided into bins of 100 atoms, and the indium content was calculated for each bin. The solid line shows the binomial distribution that would be expected in the case of a random alloy. Similar data are also available in Ref. 15.

both more diffuse and rougher.[16] In indium isoconcentration surfaces illustrating the upper interface, such as that shown in Fig. 2(a), islands one to two monolayers high and a few nanometers across were observed on the InGaN surface, and this observation was supported by other data from TEM[7] and atomic force microscopy (AFM).[16] In our model, we have included islands at the upper interface similar to those observed experimentally, since the well width fluctuations (WWFs) the islands cause have previously been predicted to significantly affect carrier localization.[5–7] We have investigated the effect of 10 nm diameter, one monolayer thick disk-shaped WWFs in our calculations, as schematically demonstrated in Fig. 2(b). We have not included interface diffuseness in our model, but since this diffuseness is homogeneous in the plane of the QW we expect this to have a less pronounced effect on the localization than the WWFs.

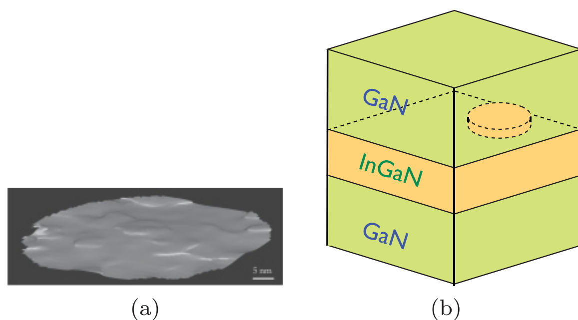

FIG. 2. (Color online) (a) An isoconcentration surface based on APT data illustrating the roughness of the upper interface of an InGaN QW. Islands one or two monolayers high and a few nanometers across are observed.[16] (b) Schematic diagram of InGaN/GaN QW with disk-shaped monolayer well width fluctuation.

II. THEORY

To investigate the localization of the carriers in these structures the carrier wave functions are calculated by solution of the effective mass Schrödinger equation. This method requires knowledge of the potential energy for the carriers. Our calculation of the potential energy of the carriers includes the effects of the band offset between InN and GaN, the spontaneous polarization, the piezoelectric field, and the deformation potential. As this potential varies spatially in all three dimensions, this potential energy can be referred to as an "energy landscape." We discuss the calculation of the potential energy in Sec. II A and the solution of the Schrödinger equation in Sec. II B. In Sec. II C we also discuss the applicability of the effective mass approximation on the length scales where we observe significant deviations from a smooth energy landscape and compare our results with those predicted by an atomistic calculation.

A. Potential energy landscape

The potential energy landscape depends critically on the distribution of indium atoms. As described above we take the indium atoms to be distributed randomly in the QW. For the continuum strain mechanics we employ, the indium distribution must be described by a smoothly varying concentration function. To calculate this concentration function we first occupy cation lattice sites with indium atoms with probability equal to the nominal concentration. We use Gaussian functions with a standard deviation equal to the cation lattice spacing to smooth this positional data. We discuss this choice of smoothing in the results section. An example of the resulting indium concentration function, $\chi(\mathbf{r})$, is shown in Fig. 3. The fluctuations in indium fraction seen in Fig. 3 arise naturally from the *random* distribution of indium atoms and are fundamental to the calculations which follow. It should be noted that the maxima of the indium concentration seen in Fig. 3 are *not* due to individual indium atoms, but instead represent the averaged effect of several indium atoms lying

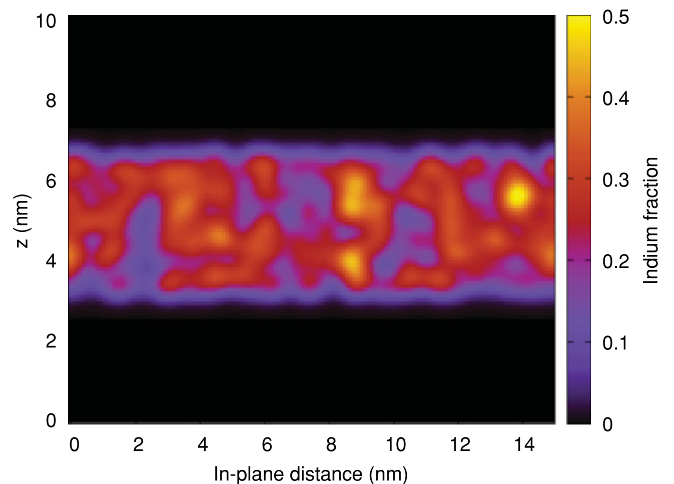

FIG. 3. (Color online) A result of our calculation of the indium fraction in a QW of width 3 nm with an average indium concentration of 25%. The z direction is normal to the x-y plane of the QW.

close to one another; this can be confirmed by examining the distance scales on the axes of the plot.

These fluctuations in local indium fraction are responsible for the local variations in quantum confinement. To calculate this locally varying band gap we use the quadratic approximation,

$$E_g(\mathbf{r}) = \chi(\mathbf{r})E_g^{\mathrm{InN}} + [1-\chi(\mathbf{r})]E_g^{\mathrm{GaN}} - b\chi(\mathbf{r})[1-\chi(\mathbf{r})]. \quad (1)$$

E_g^{InN} and E_g^{GaN} are the energy gaps in InN and GaN, respectively, and b is the bowing parameter. These parameters and all the relevant mechanical constants are taken, or derived, from Vurgaftman and Meyer's review article,[17] and the effective mass parameters are from Rinke *et al.*[18]

The strength of the spontaneous polarization which occurs in wurtzite structures also depends on the indium concentration and we describe the polarization using a linear approximation,

$$\mathbf{P}_{\mathrm{sp}}(\mathbf{r}) = \chi(\mathbf{r})\mathbf{P}_{\mathrm{sp}}^{\mathrm{InN}} + [1-\chi(\mathbf{r})]\mathbf{P}_{\mathrm{sp}}^{\mathrm{GaN}}. \quad (2)$$

We can also write this as

$$\mathbf{P}_{\mathrm{sp}}(\mathbf{r}) = \chi(\mathbf{r})\left(\mathbf{P}_{\mathrm{sp}}^{\mathrm{InN}} - \mathbf{P}_{\mathrm{sp}}^{\mathrm{GaN}}\right) + \mathbf{P}_{\mathrm{sp}}^{\mathrm{GaN}}. \quad (3)$$

As the polarization is purely in the z direction, we can write $\mathbf{P}_{\mathrm{sp}}^{\mathrm{InN}} - \mathbf{P}_{\mathrm{sp}}^{\mathrm{GaN}} = \Delta P\hat{\mathbf{z}}$. This can be used in Poisson's equation,

$$\rho_{\mathrm{sp}} = -\Delta P\frac{\partial\chi(\mathbf{r})}{\partial z} = -\nabla\cdot(\epsilon_0\epsilon_r\nabla\phi_{\mathrm{sp}}), \quad (4)$$

which, after taking the Fourier transform, gives

$$\tilde{\phi}_{\mathrm{sp}}(\mathbf{k}) = -\frac{ik_3}{\epsilon_0\epsilon_r k^2}\Delta P\tilde{\chi}(\mathbf{k}) \quad (5)$$

for the corresponding electrostatic potential. This contribution is evaluated numerically and transformed to real space using a fast Fourier transform (FFT).

Further to this the lattice constants of InN and GaN differ, so that the fluctuating indium distribution causes an inhomogeneous strain field. This strain causes a deformation potential and a large piezoelectric field. We use a Green's function method to find the strain field, and the following description closely follows that by Andreev *et al.*[19] The Green's tensor $G_{kn}(\mathbf{r})$ gives the displacement at $\mathbf{r}$ in the direction k, due to a unit point force in direction n placed at the origin. For an infinite anisotropic, homogeneous elastic medium, it is the solution to the equation[20]

$$\lambda_{ij,kl}\frac{\partial^2 G_{kn}(\mathbf{r})}{\partial x_j\partial x_l} = -\delta(\mathbf{r})\delta_{in}. \quad (6)$$

For small deformations we are then able to write an expression for the strain tensor in terms of the Green's function and concentration function, $\chi(\mathbf{r})$. We solve for the Green's function by Fourier transform and obtain an expression for the strain in Fourier space. By numerical evaluation of this function, and by performing a FFT we are able to calculate the real space strain distribution due to the inhomogeneous indium concentration function.

The deformation potential accounts for the change in energy levels due to this strain. To calculate the deformation potential the band gap energy is given in terms of the deformation potentials, D and a, and the strain tensor $\mathbf{U}$ by

$$E_g(\mathbf{U}) = E_g(0) + U_{zz}(a_1 - D_3) + (U_{xx}+U_{yy})(a_2 - D_4) \quad (7)$$

where the $\mathbf{r}$ dependance is implicit.[21]

Once we have calculated the strain in the material finding the piezoelectric field is straightforward. The polarization caused by the piezoelectric effect can be written as $p_i = e_{i,kl}U_{kl}$, where $e_{i,kl}$ is the piezoelectric tensor. Poisson's equation is solved in the same manner as for the spontaneous polarization.

B. Carrier wave functions

The carrier wave functions and energy eigenvalues are obtained by solution of the effective mass Schrödinger equation,

$$\mathcal{H}\psi(\mathbf{r}) = -\frac{\hbar^2}{2}\nabla\cdot\left[\frac{1}{m(\mathbf{r})}\nabla\psi(\mathbf{r})\right] + V(\mathbf{r})\psi(\mathbf{r}) = E\psi(\mathbf{r}), \quad (8)$$

where we use an anisotropic, inhomogeneous effective mass. The hole in-plane (perpendicular to the c axis) effective mass increases rapidly away from the band edge[22,23] and 1D calculations for the c-plane QW samples detailed below revealed holes ~15–55 meV away from the band edge. To avoid the use of prohibitively expensive iterative methods we have assumed far from the band edge hole effective masses as given by Chuang and Chang.[24]

As our potential energy $V(\mathbf{r})$ has already been evaluated numerically, it is a straightforward exercise to solve this equation using a finite difference method, with periodic boundary conditions on the wave function. The resulting sparse matrix eigenvalue problem is solved using the ARPACK subroutine library.[25] This allows us to find the lowest energy eigensolutions of the system.

In Fig. 4 we show the calculated ground state probability density of an electron (red) and a hole (green); they were calculated for a 3 nm wide 25%-indium QW, and are clearly localized on a scale of just a few nanometers. While Fig. 4 shows both hole and electron wave functions it should be noted that the interaction between them is not included in these calculations. To quantify this localization we define our localization length as $\Delta\mathbf{r}$, using the standard quantum mechanical expression

$$(\Delta\mathbf{r})^2 = \int|(\mathbf{r}-\langle\mathbf{r}\rangle)\psi|^2 d^3\mathbf{r}, \quad (9)$$

where

$$\langle\mathbf{r}\rangle = \int\mathbf{r}|\psi|^2 d^3\mathbf{r}. \quad (10)$$

C. Effective mass approximation

While the effective mass approximation (EMA) is used successfully to determine confined state energies in semiconductor heterostructures where the rapidly varying local potential in the confinement direction(s) is ignored, its use

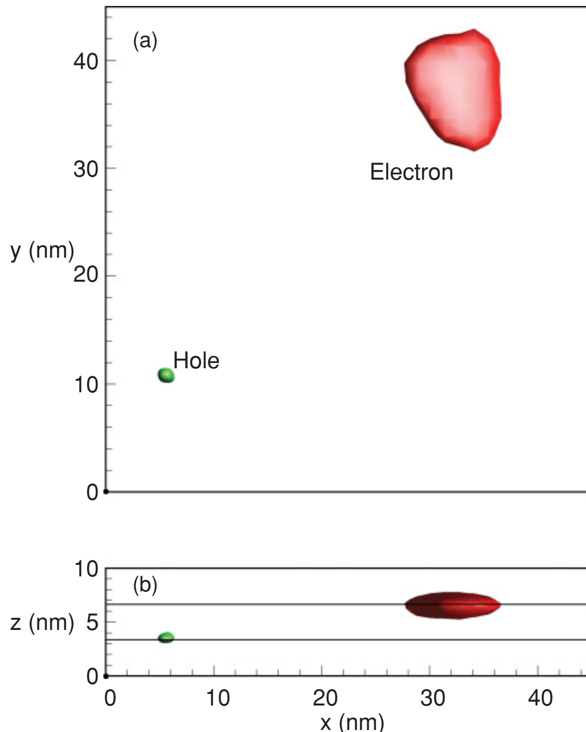

FIG. 4. (Color online) The calculated ground state probability density of an electron (red) and a hole (green). The isosurfaces are taken at one standard deviation of the maximum of the function and plotted in real space in units of nanometers. (a) The view along the z axis. (b) The view along the y axis. The plane of the QW is normal to the z axis, and the interfaces are at $z = 3.5$ and 6.5 nm.

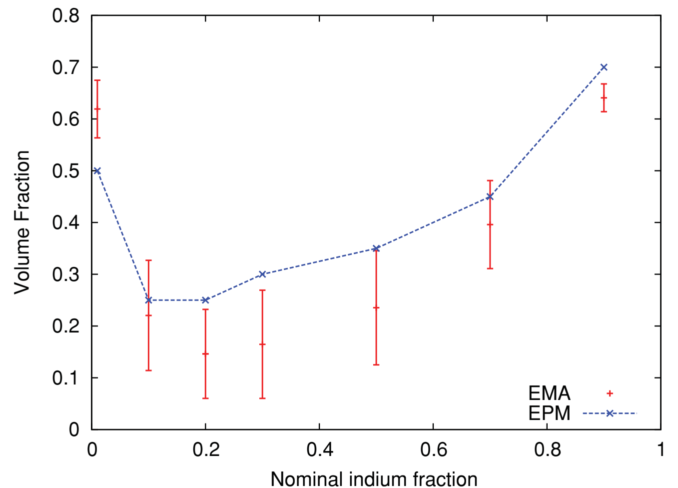

FIG. 5. (Color online) The calculated volume fraction for the charge density of the valence band maximum plotted as a function of indium fraction using EMA and EPM models. Error bars represent standard deviations.

to describe the energy landscape on a much finer length scale needs to be justified.

The local fluctuations in band gap due to the local fluctuations in indium fraction provide three-dimensional carrier confinement similar to that in self-organized quantum dot systems except on a much smaller length scale. For self-organized quantum dots the EMA can predict confined state energies that agree very well with more detailed *ab initio* atomistic calculations[26] even when the confinement is on the scale of one nanometer or less. Similarly, for wide- and narrow-gap semiconductor nanoparticles embedded in SiO_2, the EMA has predicted band gaps in good agreement with experiment, even for particle diameters in the range 1–2 nm.[27]

To provide further justification for our use of the EMA on the length scales we consider here we have compared results from our model with those derived using an empirical pseudopotential method (EPM).[28] Specifically we have calculated the valence band maxima for the same structures considered by Chan *et al.*[28] and compared the results of our calculations with those using an EPM model.

Chan *et al.*[28] determined the effect of fluctuations in the local In concentration by calculating the volume fraction of the largest contributions to 80% of the charge density. In Fig. 5 we show the volume fraction of the VBM calculated in our EMA along with the EPM results of Chan *et al.* We find quantitative agreement between our results and the atomistic EPM calculations, although the EMA tends to slightly underestimate the volume fraction. This result, though, demonstrates that the EMA with a locally varying potential is capturing the essential physics of these systems, across the entire range of indium compositions.

III. RESULTS AND DISCUSSION

To investigate the localization properties of the carriers we performed the calculations described above for different random distributions of indium atoms. Calculation system sizes of $15 \times 15 \times 10$ nm were used to find the 15 lowest energy hole states for 45 different distributions. The four lowest energy electron states were calculated in 65 larger $45 \times 45 \times 10$ nm systems owing to the larger localization lengths of these states. The systems studied were 3 nm thick QWs which varied in average indium composition between 5% and 25%. We investigate the effect of the local fluctuations in indium concentration in polar (c-plane) QWs, monolayer WWFs as described in Sec. I, and matching nonpolar (a- or m-plane) samples.

The mean localization lengths $\Delta \mathbf{r}$, as defined in Eq. (9), for the lowest energy hole and electron eigenstates are plotted against the nominal indium fraction in Figs. 6(a) and 6(b), respectively. Considering the effects of indium fluctuations only, the hole wave functions show a constant localization length of $\sim$1.0 nm across the range of indium concentrations. The electrons show an increasing localization length from $\sim$7 nm for the 25% indium sample to $\sim$10 nm for the 5% indium sample. This trend of increasing localization length with decreasing nominal indium concentration is caused by the reduction in magnitude of the fluctuations (the standard deviation of the concentration distribution decreases) as the nominal concentration gets smaller. The holes do not display this behavior as the larger hole effective mass means they are less sensitive to the changing depth of fluctuations. The difference in overall localization length scale can also be attributed to the difference in the effective mass between the electrons and holes.

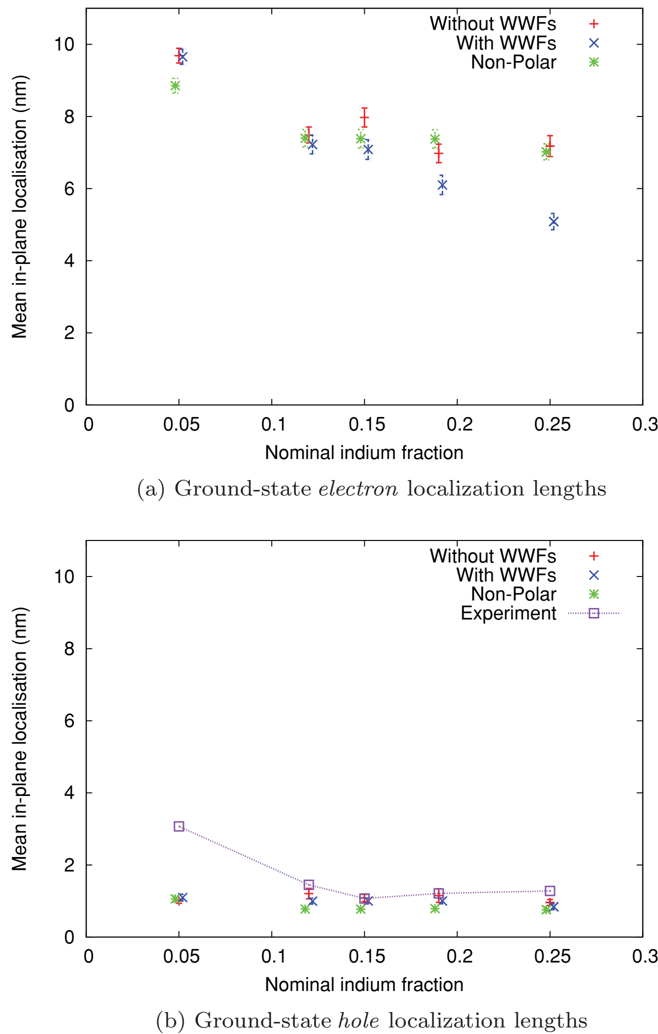

(a) Ground-state *electron* localization lengths

(b) Ground-state *hole* localization lengths

FIG. 6. (Color online) Mean ground-state localization lengths are shown for QWs of different indium fraction, with and without WWFs and in a nonpolar orientation. (a) Electron localization lengths. (b) Hole localization lengths with data from Graham *et al.*[7] also plotted for comparison. Error bars represent the standard error.

We consider the effect of our choice of smoothing parameter on the results presented above. It should first be understood that the value $\sigma_{xy} = 1.0\,a$ already represents a very considerable degree of smoothing: When an array of delta functions with spacing a is convolved with a Gaussian function with $\sigma = a$, the smoothed distribution is uniform to within $\pm 5.4 \times 10^{-9}$. If a much larger value of the smoothing parameter, $\sigma_{xy} = 2.0\,a$, is used in our calculations, we find that this leads to no appreciable change in the electron localization lengths and that the hole localization lengths are increased by less than 40%; such an effect on the holes is to be expected, as the smoothing length scale is now comparable with the hole localization length. So, although the choice of smoothing affects the precise value of the calculated hole localization lengths, the degree of localization remains high, and the mechanisms that lead to localization are unchanged. In Sec. II C, we have shown that our results for the volume fraction occupied by localized states agree well with those of an atomistic calculation, and this gives independent support for our particular choice of smoothing parameter, $\sigma_{xy} = 1.0\,a$.

When we consider the added contribution of WWFs on the carrier localization lengths we see a marked difference in their effect on electrons and holes. The mean localization length for the electrons in the 25% indium sample is reduced by a third with the introduction of this WWF, whereas for the holes the WWF has almost no effect on the localization. This difference arises from the effect of the electric field, which causes the holes to be localized on the smoother (lower) interface, and the electrons to be localized on the rougher (upper) interface. It should be noted that the holes are localized on a shorter length scale than the WWF. The effect of the large electric field across the QW was investigated by comparing the polar results with calculations on QWs in a nonpolar (*a*- or *m*-plane) orientation. For the polar QWs we have neglected the excitonic interaction, which is justified in wide wells due to the separation of the carriers caused by the electric field. This is not the case in nonpolar QWs; nevertheless the calculations provide at least qualitative information about carrier localization in such structures. We also only consider the effect of alloy fluctuations in this orientation, not WWFs. We see that again the hole localization lengths are unchanged throughout the range of concentrations investigated. The electron localization is also unchanged, suggesting the electric field has little effect on carrier localization. At this stage we have not yet considered the effect of the electric field on electron localization in the presence of WWFs. We have also compared our results with the localization lengths of Graham *et al.*[7] in Fig. 6(a). They obtained Huang-Rhys factors from the strength of the LO-phonon replicas in PL spectra at low temperature and compared these with the results of calculations which assumed Gaussian wave functions for the localized carriers. This allowed them to estimate the carrier localization lengths. These show encouraging agreement with our hole localization results, which may demonstrate that the relevant

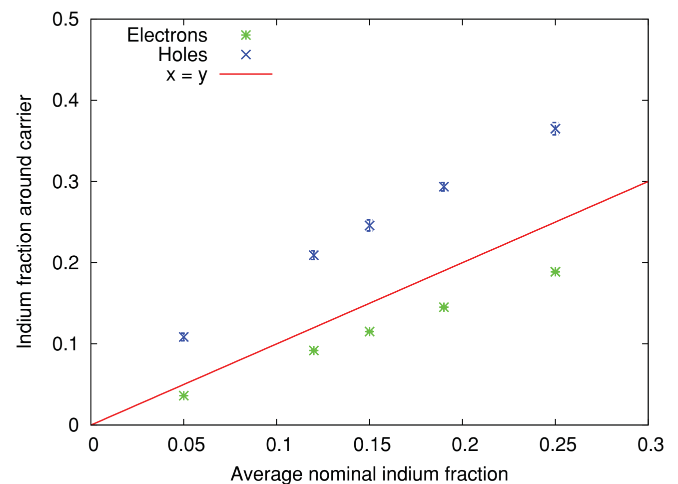

FIG. 7. (Color online) The mean indium fraction within one standard deviation of the maximum of the electron and hole probability densities is plotted against the nominal indium fraction of the QW. Error bars represent the standard error in the mean.

localization length being probed in the experiment is that of the holes.

Considering only the polar QWs with no WWFs, Fig. 7 shows the mean indium fraction in the neighborhood of the localized carriers for each nominal concentration. We are able to calculate this by comparing the local concentration function for the sample with the calculated wave functions, and take the neighborhood of the carrier to be within one standard deviation of the peak of the wave function. Figure 7 clearly indicates that the holes are localized in naturally occurring regions of higher indium concentration. In the nominally 25% sample for example, the mean indium concentration under the lowest energy hole wave functions was 37%. It should once again be noted that these regions with above average indium content occur due to random fluctuations in composition. The mean indium concentration around the electrons in this sample was approximately 19%. This is lower than the nominal concentration as the electron wave functions penetrate into the GaN barrier.

We can approximate the localization energies of the carriers by fitting the density of localized states with stretched exponentials,

$$g_{e/h}(E) \approx n_0 \exp\left[-\left(\frac{|E-E_{e/h}|}{\sigma}\right)^a\right], \tag{11}$$

where $a = 1.5$ for the holes and $a = 2$ for the electrons. We find the localization energy (σ) of the holes in the 25% indium c-plane sample without WWFs to be ~55 meV, and ~11 meV for the electrons. This again emphasizes the stronger localization of the holes in these structures.

All of our results point toward a picture of localization in which the holes are strongly localized by statistical fluctuations in indium concentration, and electrons are localized on a longer length scale by a combination of these alloy fluctuations and well width fluctuations. This picture may, however, be changed if the Coulomb interaction between carriers leads to the binding of electrons to the strongly localized holes; we have not attempted to include such effects in the work presented here.

Our calculations allow us to determine the oscillator strengths and energies of photons emitted during recombination. To ensure that we included all of the localized hole states within a given sample, we performed the calculation in a slightly smaller system, and calculated more states. We calculated 4 of the lowest energy electron states in 50 $48 \times 48 \times 10$ nm samples, and 35 hole states in 800 $12 \times 12 \times 10$ nm samples. We approximate the low temperature PL spectra of the samples by assuming that the localized states are all occupied by carriers, and by convolving the discrete recombinations with Gaussians of standard deviation 7 meV. This width is chosen to be small enough for it not to affect the width of the final spectrum, but large enough for the spectrum to be relatively smooth. Note that due to the finite size of the system there will be long wavelength fluctuations in the indium concentration which are neglected. The effect of these would be to broaden the low energy tail slightly. Comparison of our calculated PL spectrum for a single 3.3 nm thick 25% indium QW with no WWFs with an experimental PL spectrum of a nominally identical sample is shown in Fig. 8. The widths of the peaks, often attributed to localization effects, compare very well: The simulated PL has a FWHM of 69 meV, and the FWHM of the experimental PL is 63 meV. In our calculations the strong hole localization is the cause of this broadening. The low energy features in the experimental PL are LO-phonon replicas of the main peak and do not appear in the simulated spectrum as we have not included the electron-phonon interaction in our calculations. Including the effects of WWFs increases this broadening on the low energy side of the peak, but the effect is much smaller than that caused by the hole localization. With allowance for the uncertainty in the experimental determination of, for example, the piezoelectric coefficients, the peak energies also agree reasonably well.

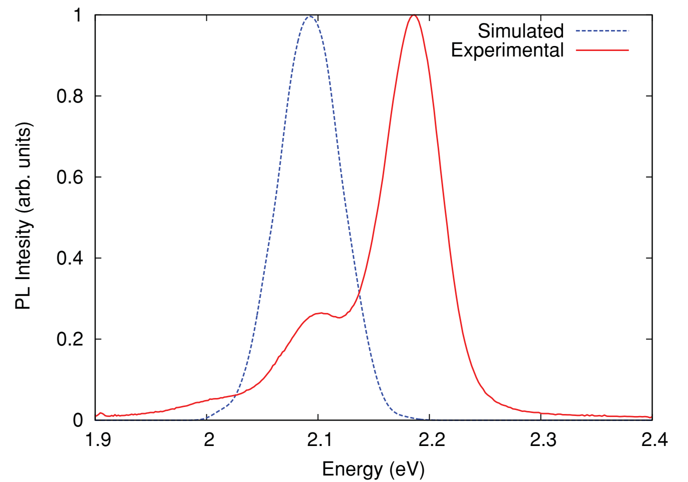

FIG. 8. (Color online) A simulated PL spectrum for a 25% indium single QW with no WWFs, compared with low temperature experimental PL spectra reported by Graham *et al.*[7] The low energy feature of the experimental PL spectra are LO-phonon replicas of the main peak; the electron-phonon interaction is not included in the simulated spectrum.

IV. SUMMARY

We have been able to build a picture of the localization of the carriers in InGaN/GaN QWs by performing effective mass calculations for different random distributions of indium atoms. We have found that the holes are strongly localized in regions of above average indium content. The electrons are less strongly localized by the indium fluctuations, but become more localized by mono-layer well width fluctuations. Our work demonstrates carrier localization without the need for gross indium clusters, which goes some way to explaining the carrier localization mechanisms which are so important for the operation of InGaN optoelectronic devices.

ACKNOWLEDGMENTS

We acknowledge the financial support by the UK Engineering and Physical Sciences Research Council, Grants No. EP/E035191/1 and No. EP/E035167/1. R.A.O. would like to acknowledge financial support from the Royal Society.

*duncan.parris@postgrad.manchester.ac.uk

[1] S. Nakamura, Science **281**, 956 (1998).
[2] S. Chichibu, K. Wada, and S. Nakamura, Appl. Phys. Lett. **71**, 2346 (1997).
[3] K. L. Teo, J. S. Colton, P. Y. Yu, E. R. Weber, M. F. Li, W. Liu, K. Uchida, H. Tokunaga, N. Akutsu, and K. Matsumoto, Appl. Phys. Lett. **73**, 1697 (1998).
[4] J. Davidson, P. Dawson, T. Wang, T. Sugahara, J. Orton, and S. Sakai, Semicond. Sci. Technol. **15**, 497 (2000).
[5] N. Grandjean, B. Damilano, and J. Massies, J. Phys. Condens. Matter **13**, 6945 (2001).
[6] S. Dhar, U. Jahn, O. Brandt, P. Waltereit, and K. H. Ploog, Phys. Status Solidi A **192**, 85 (2002).
[7] D. M. Graham, A. Soltani-Vala, P. Dawson, M. J. Godfrey, T. M. Smeeton, J. S. Barnard, M. J. Kappers, C. J. Humphreys, and E. J. Thrush, J. Appl. Phys. **97**, 103508 (2005).
[8] D.-P. Nguyen, N. Regnault, R. Ferreira, and G. Bastard, Solid State Commun. **130**, 751 (2004).
[9] L. Bellaiche, T. Mattila, L.-W. Wang, S.-H. Wei, and A. Zunger, Appl. Phys. Lett. **74**, 1842 (1999).
[10] D. Gerthsen, E. Hahn, B. Neubauer, A. Rosenauer, O. Schön, M. Heuken, and A. Rizzi, Phys. Status Solidi A **177**, 145 (2000).
[11] Y.-C. Cheng, E.-C. Lin, C.-M. Wu, C. C. Yang, J.-R. Yang, A. Rosenauer, K.-J. Ma, S.-C. Shi, L. C. Chen, C.-C. Pan *et al.*, Appl. Phys. Lett. **84**, 2506 (2004).
[12] T. M. Smeeton, M. J. Kappers, J. S. Barnard, M. E. Vickers, and C. J. Humphreys, Appl. Phys. Lett. **83**, 5419 (2003).
[13] L.-W. Wang, Phys. Rev. B **63**, 245107 (2001).
[14] P. R. C. Kent and A. Zunger, Appl. Phys. Lett. **79**, 1977 (2001).
[15] M. J. Galtrey, R. A. Oliver, M. J. Kappers, C. J. Humphreys, D. J. Stokes, P. H. Clifton, and A. Cerezo, Appl. Phys. Lett. **90**, 061903 (2007).
[16] M. J. Galtrey, R. A. Oliver, M. J. Kappers, C. J. Humphreys, P. H. Clifton, D. Larson, D. W. Saxey, and A. Cerezo, J. Appl. Phys. **104**, 013524 (2008).
[17] I. Vurgaftman and J. R. Meyer, J. Appl. Phys. **94**, 3675 (2003).
[18] P. Rinke, M. Winkelnkemper, A. Qteish, D. Bimberg, J. Neugebauer, and M. Scheffler, Phys. Rev. B **77**, 075202 (2008).
[19] A. D. Andreev, J. R. Downes, D. A. Faux, and E. P. O'Reilly, J. Appl. Phys. **86**, 297 (1999).
[20] L. Landau and E. Lifshitz, *Theory of Elasticity*, Landau and Lifshitz Course of Theoretical Physics, Vol. 7 (Pergamon, Oxford, 1986), 3rd ed.
[21] J.-M. Wagner and F. Bechstedt, Phys. Rev. B **66**, 115202 (2002).
[22] P. A. Shields, R. J. Nicholas, F. M. Peeters, B. Beaumont, and P. Gibart, Phys. Rev. B **64**, 081203 (2001).
[23] K. Kim, W. R. L. Lambrecht, B. Segall, and M. van Schilfgaarde, Phys. Rev. B **56**, 7363 (1997).
[24] S. L. Chuang and C. S. Chang, Phys. Rev. B **54**, 2491 (1996).
[25] R. B. Lehoucq, D. C. Sorensen, and C. Yang, *ARPACK Users' Guide: Solution of Large-Scale Eigenvalue Problems with Implicitly Restarted Arnoldi Methods* (SIAM, 1998).
[26] B. Delley and E. F. Steigmeier, Appl. Phys. Lett. **67**, 2370 (1995).
[27] K. K. Nanda, F. E. Kruis, H. Fissan, and S. N. Behera, J. Appl. Phys. **95**, 5035 (2004).
[28] J. A. Chan, J. Z. Liu, and A. Zunger, Phys. Rev. B **82**, 045112 (2010).